Coupling a Single-Layer Urban Canopy Model with a Simple Atmospheric Model: Impact on Urban Heat Island Simulation for an Idealized Case

Hiroyuki KUSAKA

Fluid Science Department, Central Research Institute of Electric Power Industry, Japan

and

Fujio KIMURA

Institute of Geoscience, University of Tsukuba, Japan

(Manuscript received 14 January 2003, in final form 25 September 2003)

Abstract

We incorporated a single-layer urban canopy model into a simple two-dimensional atmospheric model in order to describe the fundamental impact of the urban canopy model on an idealized urban heat island simulation. We found that the heat island circulation developed less strongly than when using the atmospheric model with the standard slab urban model. Additionally, the coupling with urban canopy model (i) delays the phase of surface air temperature, (ii) reduces the diurnal range of the temperature, and (iii) produces a nocturnal heat island, which results from the difference in atmospheric stability between city and its surroundings. The features from the atmospheric model coupled with the canopy model agree well with those from observation, although the atmospheric model with the slab model does not. The simulated nocturnal heat island is caused by the larger heat storage of the canopy model which releases sensible heat after sunset.

1. Introduction

Surface-layer in cities is generally warmer than that of their surroundings. Near a city, the surface isotherms looks like the topographic contours around an island. Thus, this phenomenon has become known as the urban heat island, which is clearly observed under atmospheric conditions of a clear sky and light wind. In particular, it is most pronounce in winter. Thus, most studies have traditionally focused on the winter season. Recently, the importance of the heat island in summer has been recognized in relation to several problems including uncomfortable conditions and high energy demand.

Numerical simulations under idealized or realistic summer synoptic conditions have been conducted using two- or three-dimensional mesoscale models that include a standard surface-layer scheme called slab urban model (e.g., Kimura and Takahashi 1991; Yoshikado 1992, 1994; Avissar 1996; Ichinose et al. 1999; Kusaka et al. 2000; Kanda et al. 2001; Ohashi and Kida 2002a, 2002b). Their numerical studies have provided us with important and essential idea of the urban weather and climate in summer. However, we still need to continue

Corresponding address: Mesoscale and Micoroscale Meteorology Division, National Center for Atmospheric Research, 3450 Mitchell Lane, Boulder, CO 80301, USA.
E-mail: kusaka@ucar.edu
© 2004, Meteorological Society of Japan

urban modeling and increase the accuracy of the surface energy balance, in order to improve weather forecasts, estimate energy consumption, aid in urban planning, and for better understanding of the urban weather and climate.

An approach using a multi-layer urban canopy model is suitable for studying the temperature and wind profiles within urban canopy layer or boundary layer; however, it needs much higher spatial resolution than that of current mesoscale models (e.g., Uno et al. 1989; Kondo et al. 1999; Ca et al. 2002; Martilli et al. 2002). Single-layer urban canopy models have been also proposed by Mills (1997), Masson (2000), and Kusaka et al. (2001). Their canopy models can be easily applied to mesoscale models without modifying the dynamic core. Kusaka et al. (2001) confirmed that surface temperatures and net radiation calculated from their model agreed closely with the observed ones. Additionally, the performance of their model is nearly that of the multi-layer model for the surface fluxes which are important for the study of the mesoscale urban heat island.

In this study, we incorporate the single-layer urban canopy model into a simple two-dimensional atmospheric model, and present its impact on the heat island and atmospheric circulation. Note that the present simulations are conducted under an ideal condition using a simple mesoscale model. Such a simulation provides us comprehensible results necessary for a step toward a real case. Indeed, Kimura (1989), Uno et al (1995), and Avissar and Pielke (1989) investigated the impact of their proposed surface parameterization under the simple model condition mentioned above. It is also noteworthy that the present study does not investigate the effects on the microscale flow and thermal environment.

A brief description of the numerical atmospheric model, and single-layer urban canopy model is given in Section 2. The results of simulations are shown in Section 3. Discussion and conclusion follow in Sections 4 and 5, respectively.

2. Model description

2.1 Local circulation models

The atmospheric model used in the present study is *x-z* two-dimensional Local Circulation Model (e.g., Kimura and Manins 1988; Kimura and Kuwagata 1993, 1995; Lee and Kimura 2001). However, in the present model, the soil temperature is calculated by a multi-layer heat equation model, which solves the vertical diffusion equation, instead of the Force-Restore method. We call this version LCM2D. Furthermore, the present study couples the LCM2D with the modified version of the single-layer urban canopy model developed by Kusaka et al. (2001). We call the version LCM2D-C. The following is a brief description of LCM2D and LCM2D-C.

The anelastic equations of motion based on the hydrostatic assumption are

$$\frac{\partial u}{\partial t} + u\frac{\partial u}{\partial x} + w\frac{\partial u}{\partial z} = fv - \Theta\frac{\partial \pi'}{\partial x} + \frac{\partial}{\partial x}\left(K_H\frac{\partial u}{\partial x}\right) + \frac{\partial}{\partial z}\left(K_m\frac{\partial w}{\partial z}\right), \quad (1)$$

and

$$\frac{\partial v}{\partial t} + u\frac{\partial v}{\partial x} + w\frac{\partial v}{\partial z} = -f(u - u_G) + \frac{\partial}{\partial x}\left(K_H\frac{\partial v}{\partial x}\right) + \frac{\partial}{\partial z}\left(K_m\frac{\partial w}{\partial z}\right). \quad (2)$$

The hydrostatic equation is

$$\frac{\partial \pi'}{\partial z} = g\frac{\theta'}{\Theta^2}, \quad (3)$$

and the continuity equation is

$$\frac{\partial \rho_0 u}{\partial x} + \frac{\partial \rho_0 w}{\partial z} = 0. \quad (4)$$

The thermodynamic equation is expressed as

$$\frac{\partial \theta'}{\partial t} + u\frac{\partial \theta'}{\partial x} + w\frac{\partial \theta'}{\partial z} = \frac{\partial}{\partial x}\left(K_H\frac{\partial \theta'}{\partial x}\right) + \frac{\partial}{\partial z}\left(K_h\frac{\partial \theta'}{\partial z}\right) + Q_{RCOOL}, \quad (5)$$

and the equation for specific humidity as

$$\frac{\partial q_v}{\partial t} + u\frac{\partial q_v}{\partial x} + w\frac{\partial q_v}{\partial z} = \frac{\partial}{\partial x}\left(K_H\frac{\partial q_v}{\partial x}\right) + \frac{\partial}{\partial z}\left(K_h\frac{\partial q_v}{\partial z}\right). \quad (6)$$

The symbols have their conventional meaning and are defined in the Appendix.

The vertical exchange coefficients are calculated in the turbulent closure model at Level 2 developed by Mellor and Yamada (1974), which has an approximate balance between production and dissipation terms of the turbulence kinetic energy equation.

Newtonian cooling is assumed in the lower atmosphere when the atmospheric temperature is less than the surface temperature. The cooling term Q_{RCOOL} is given by

$$Q_{RCOOL} = \gamma_{RCOOL}(T - T_{RAD}). \quad (7)$$

Here T is the atmospheric temperature at each level and T_{RAD} is the surface temperature, which is calculated using the upward long wave radiation on the grid. The cooling coefficient γ_{RCOOL} is assumed to be 10^{-5} sec^{-1} after Yamamoto (1973).

The top boundary is controlled by the wave radiation condition discussed in Klemp and Durran (1983), in order to avoid the reflection of gravity waves generated in lower layers. For the lateral boundaries, periodic boundary condition is applied. The lower boundary is given by the surface fluxes from the land surface models.

2.2 Single-layer urban canopy model

Land surface models are linked with atmospheric model though the surface fluxes as mentioned in Section 2.1 LCM2D uses the slab urban model (Fig. 1a) and slab grassland model for artificial and natural surfaces, respectively. These models consist of (a) the traditional surface-layer scheme using Monin-Obukhov similarity theory to estimate surface fluxes (e.g., Kimura 1989; Kusaka et al. 2000), (b) a surface energy balance equation, and (c) multi-layer heat equation model to calculate surface and soil temperatures.

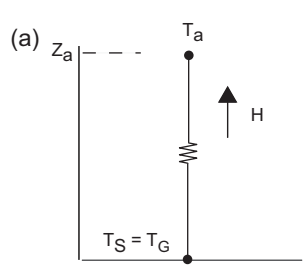

Fig. 1. (a) Slab urban model (surface layer scheme for bare soil ground).

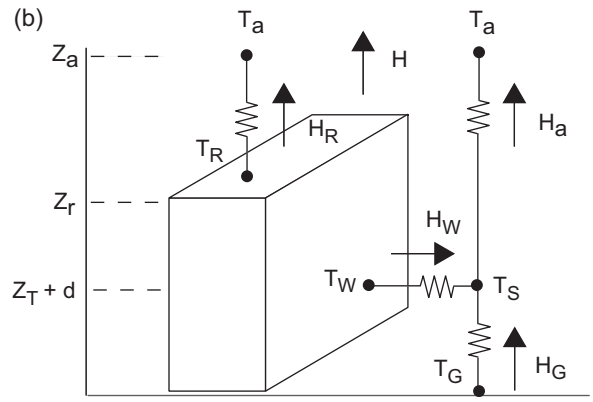

Fig. 1. (b) Schematic of the single-layer urban canopy model. T_a is the air temperature at reference height z_a, T_R the building roof temperature, T_W the building wall temperature, T_G the road temperature, and T_S the temperature defined at $z_T + d$. H is the sensible heat exchange at the reference height. H_a is the sensible heat flux from the canyon space to the atmosphere, similarly, H_W is that from wall to the canyon space, H_G that from road to the canyon space, and H_R that from roof to the atmosphere.

On the other hand, LCM2D-C uses single-layer urban canopy model (Fig. 1b) instead of slab urban model for artificial surface. The latter urban canopy model includes (a) street canyons that are parameterized to represent the urban geometry, (b) shadowing from buildings and reflection of radiation (Fig. 2), (c) the canyon orientation and diurnal change of solar azimuth angle, (d) artificial surface consists of eight canyons with different orientation (e) Inoue's model for canopy flows (Inoue 1963), (f) the multi-layer heat equation for the roof, wall, and road interior temperatures, and (g) the very thin bucket model for hydrological processes. Note that the moisture availability is determined by the type of land-cover, but is time-independent to compare with LCM2D in the present study.

This urban canopy model estimates both the surface temperatures of, and heat fluxes from the roof, wall, and road; it also calculates the energy and momentum exchange between the urban surface and the atmosphere. Addition-

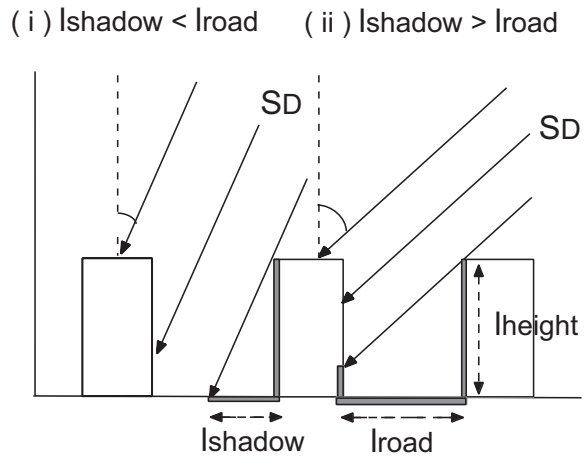

Fig. 2. Radiation of the single-layer urban canopy model. S_D is the direct solar radiation incident on a horizontal surface. l_{road} is the normalized road width and h_c is the normalized building height ($l_{roof} + l_{road} = 1$). l_{shadow} is the normalized shadow length on the road.

ally, the model uses sub-grid parameterization for heterogeneous surfaces proposed by Kimura (1989) and Avissar and Pielke (1989) because the model has two different land-cover, artificial and natural one, in a grid. Note that their parameterizations consider the area ratio of the land-cover, not the distribution. This parameterization allows the results from the canopy model to be compared with those from operational observation, which is carried out above grass-covered open space in cities. More details about the present canopy model are described in the Appendix B.

3. Impacts of the single-layer urban canopy model on the heat island simulation

3.1 Simulation domain and initial condition

It is important to investigate the impacts of the single-layer urban canopy model on a mesoscale simulation because a land surface model provides the lower boundary condition of an atmospheric model. Simulations were produced using both LCM2D and LCM2D-C.

Both models were set up over a domain 300 km across and about 4 km high. The numbers of grid points were 100×29. Thus, the horizontal resolution was 3 km and the vertical resolution was 20 m near the ground, but up to 400 m at the top. Two different surface types were specified. The urban area, which is represented by 10 grid elements, is located in the middle of the simulation domain. This area is assumed to have both artificial and natural surfaces. The artificial surface occupies 80% and the natural surface 20% in the grid of the urban area. The surrounding rural areas are assumed to be only the natural surface.

Canyon dimensions and surface parameters for the single-layer urban canopy model are shown in Table 1, using Sugawara (2001) and Kusaka et al. (2001) as reference. The parameters needed for the slab urban model ($\rho c, \lambda, z_0, B_H, \varepsilon, \beta$) are the same as those used in the canopy model, based on the purpose of this study. Note that the slab model has the proper bulk albedo α which was estimated from the canopy model because the solar radiation is the one of the forcing for the urban models. Surface fluxes in the individual land-cover are averaged using the sub-grid mosaic parameterization of Kimura (1989).

The purpose of this study is to compare a standard slab urban model to a single-layer urban canopy model. Thus, it is desirable to set the same initial and boundary conditions in all simulations. Numerical integration of all simulations started at 0300 LST on the idealized summer day, August 1st , under the following weather conditions: (1) no gradient wind, and (2) a clear sky. It is considered that these are necessary conditions for the appearance of a clear urban heat island and thermally induced atmospheric circulation. The following idealized initial conditions are created from observations under such a condition (Kusaka et al. 2000). A potential temperature lapse rate of 0.005 K km^{-1} were assumed in the model atmosphere, and a relative humidity of 70% and a wind speed of 0 m s^{-1} were assumed at all levels. The model atmosphere is assumed to be horizontally homogeneous at initialization. The models were then run for 36 hours. In a calm basic state, as the time integration proceeds, the thermally induced local circulation grows. In nature, large-scale winds periodically advect the heat, and consequently produce the typical atmospheric condition like an initial condition assumed in the present study. In the model, however, such an effect could not be included.

Table 1. Canyon dimensions and surface parameters.

Parameter	Symbol	Value	Unit
Roof level (building height)	z_r	6	[m]
Normalized building height	h_c	0.35	
Normalized roof width	l_{roof}	0.3	
Normalized road width	l_{road}	0.7	
Volumetric heat capacity of artificial and natural surfaces	ρc	2.01×10^6	[J m^{-3} K^{-1}]
Thermal conductivity of artificial and natural surfaces	λ	2.28	[W m^{-1} K^{-1}]
Sub-layer Stanton number of artificial and natural surfaces	B_H^{-1}	6	
Roughness length above canyon	z_{0C}	0.667	[m]
Roughness length above roof	z_{0R}	0.005	[m]
Zero plane displacement height above artificial surface	d_A	2.3	[m]
Roughness length above natural surface	z_{0N}	0.1	[m]
Zero plane displacement height above natural surface	d_N	0	[m]
Albedo for roof surface	α_R	0.2	
Albedo for wall surface	α_W	0.2	
Albedo for road surface	α_G	0.2	
Albedo for natural surface	α_N	0.2	
Emissivity for roof surface	ε_R	0.97	
Emissivity for wall surface	ε_W	0.97	
Emissivity for road surface	ε_G	0.97	
Emissivity for natural surface	ε_N	0.97	
Canyon orientation	θ_{can}	$n\pi/8$ $(n = 1\sim8)$	[rad]
Moisture availability for artificial surface	β_A	0	
Moisture availability for natural surface	β_N	0.3	

Yoshikado (1992, 1994) and Ohashi and Kida (2002b) examined results of the 1st day from 2D simulation under similar atmospheric conditions, based on the same reason. In the present case, results of the 1st and 2nd days after initial time are examined. Anthropogenic heating can be a dominant factor for cities where energy consumption is enormous and net radiation is low, e.g., in commercial and heavy industrial areas. However, this heating is not considered in the present model so that we have to focus on the effects of the urban canopy model. Coriolis parameter is also set to zero to simplify the simulation.

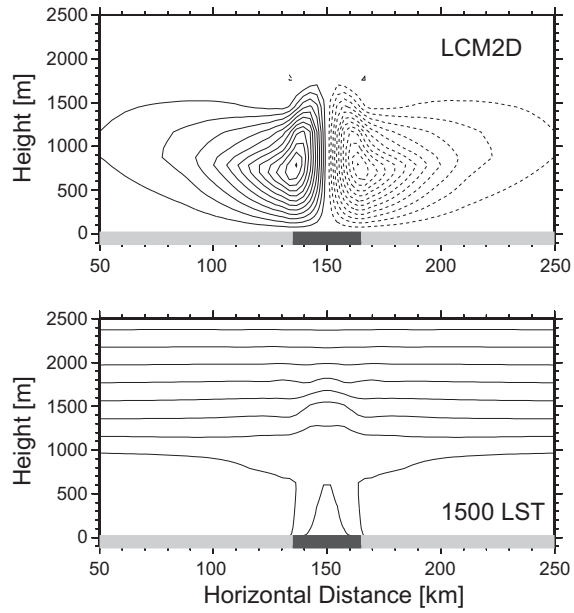

Fig. 3. Streamlines (top) and potential temperature (bottom) at 1500 LST for LCM2D, the two-dimensional local circulation model. The contour interval for the streamlines is 400 m^2 s^{-1}. The contour interval for the potential temperatures is 1 K.

3.2 *Simulated results*

a. *Heat island*

Figure 3 is the streamline-contours (top) and potential temperature-contours (bottom) at 1500 LST (12 hours after starting the numerical integration) from LCM2D. Although turbulent mixing of the atmosphere tends to obscure the influence of urban-rural daytime surface temperature differences in air temperatures, the net daytime urban impact on the atmosphere is large. The change of surface type near the center of the simulation induces the heat

island circulation, which is inward toward the central part of the urban area at lower levels, and outward from the central part of the urban area at upper levels. The horizontal flow causes a strong upward flow in a narrow region near the central part of the urban area.

The potential temperature is nearly constant with height to 800 m and a shallow mixed layer is formed over the rural areas at 1500 LST. Over the urban area, a deep mixed layer of 1200 m depth develops due to the higher surface temperature and the upward flow from the heat island circulation. Surface air temperature in the urban area is about 32°C, and the heat island intensity, which is defined as the difference in the surface air temperature between urban and rural site, is about 2°C. Figures 4a–c show the time variation of the vertical profile of potential temperature from LCM2D. After sunset (Fig. 4b), a stable layer develops due to radiative cooling in both the urban and rural sites. The heat island intensity is about 0.4°C, and the thickness is less than 50 m. At 0300 LST (Fig. 4c), the stable layer is stronger in both the urban and rural sites. The heat island intensity at this time is less than 0.4°C, which is much weaker than that at 1500 LST.

When LCM2D-C was used instead of LCM2D, the two-dimensional streamline contours show that the circulation weakens (Fig. 5). For example, by 1500 LST, the heat island circulation from LCM2D-C is similar to that from LCM2D (Fig. 3 versus Fig. 5) however, the circulation has not developed as strongly as that from LCM2D. In addition the height of the mixed layer is lower than that from LCM2D, and the heat island intensity is about 1°C, which is not as strong as that from LCM2D.

Figure 6 shows the time variation of the vertical profile of potential temperature from LCM2D-C. After sunset (2100 LST), a mixed layer is maintained in the urban site, even while a stable layer exists in the rural site. The difference in the surface air temperature between urban and rural sites shows that the heat island intensity is about 2°C, which is stronger than that from LCM2D. In addition, the intensity of the nocturnal heat island is stronger than that of the daytime heat island because at night the vertical extent of the large temperature anomaly is confined to a depth of

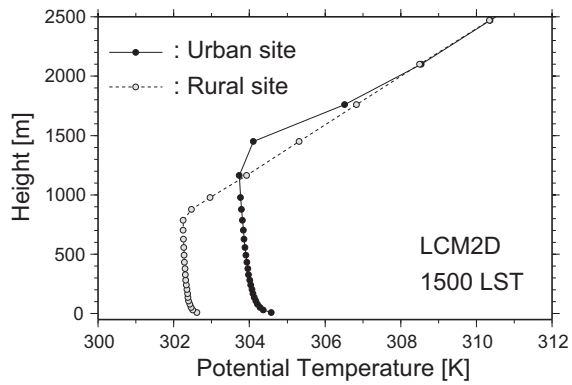

Fig. 4. (a) Vertical profile of potential temperature at 1500 LST for the two-dimensional local circulation model, LCM2D. Solid line with solid circles is the potential temperatures above urban area. Dashed line with open circles is the potential temperatures at rural site 90 km from the center of the urban area (60-km from the lateral boundary).

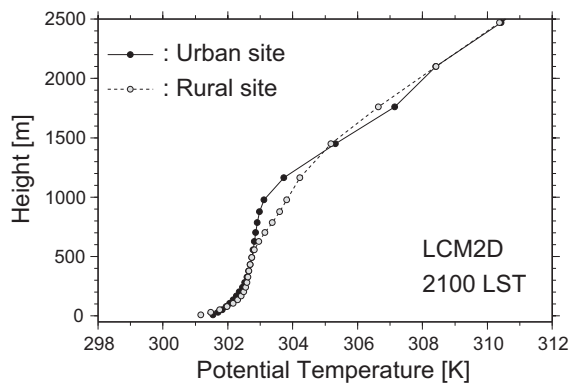

Fig. 4. (b) Same as Fig. 4a, but for 2100 LST.

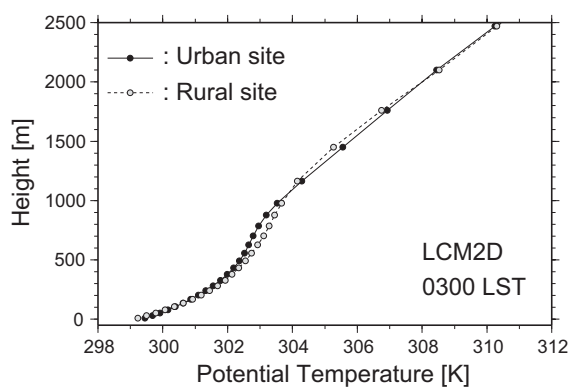

Fig. 4. (c) Same as Fig. 4a, but for 0300 LST.

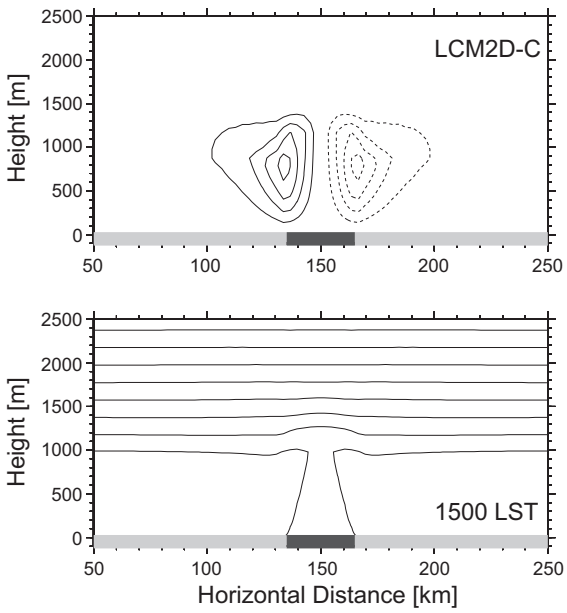

Fig. 5. Same as Fig. 3, but for LCM2D-C, the two-dimensional local circulation model coupled with the single-layer urban canopy model.

0–300 m as compared with a depth exceeding 1000 m during the day. At 0300 LST, a stable layer develops in the urban site, and thus both sites are now stable. However, the atmospheric stability in the urban site is weaker than that in the rural site.

Diurnal variations of the urban surface air temperature from LCM2D and LCM2D-C are shown in Fig. 7. The cooling rate from LCM2D is strongest during the first several hours after sunset. Thereafter, it decreases to approach the weaker urban cooling rate. On the other hand, the cooling rate from LCM2D-C is nearly constant. These cooling trends from LCM2D-C agree qualitatively with the feature of the previous observational results (e.g., Oke 1987, Yoshino and Yamashita 1998).

b. Surface heat budget

The nocturnal heat island clearly appeared using LCM2D-C. When the results of the heat budget are shown with respect to the heat island intensity, the formation mechanism of the heat island by LCM2D-C become clear. Figures 8 and 9 show some differences in a diurnal variation of surface energy budget between ur-

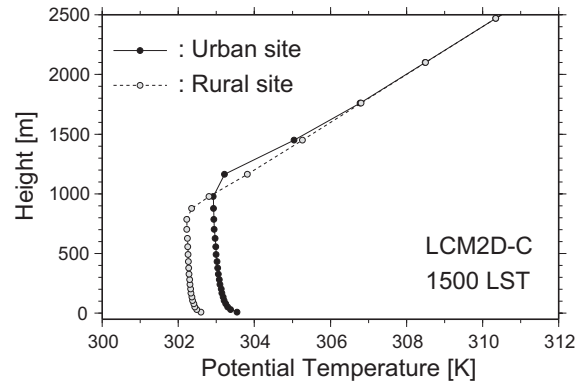

Fig. 6. (a) Same as Fig. 4a, but for LCM2D-C.

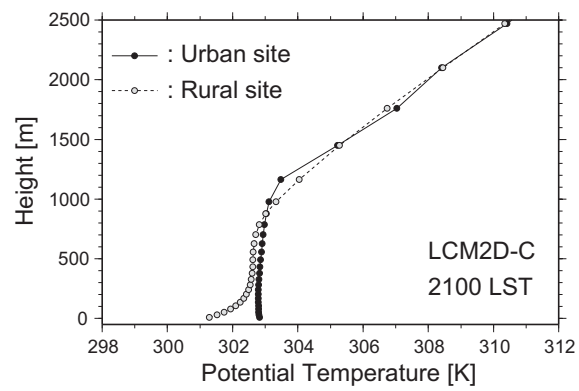

Fig. 6. (b) Same as Fig. 4b, but for LCM2D-C.

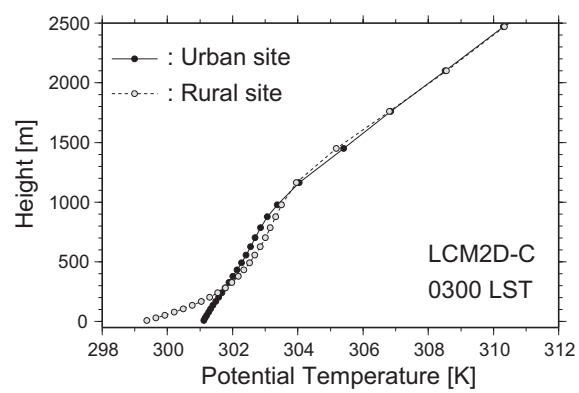

Fig. 6. (c) Same as Fig. 4c, but for LCM2D-C.

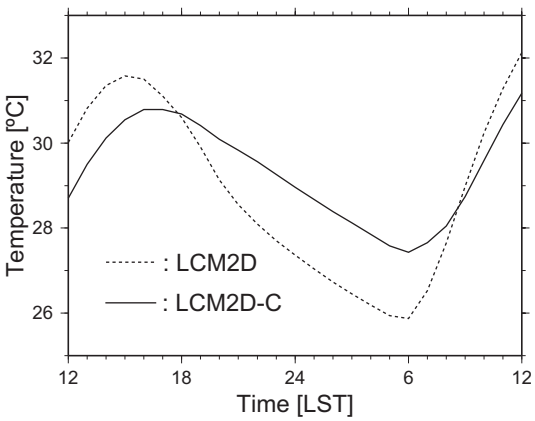

Fig. 7. Diurnal variation of surface air temperature from LCM2D and LCM2D-C. The dashed line is from LCM2D and the solid line is from LCM2D-C. Location is the urban site, the center of the urban area. Sunrise is at 0517 LST and Sunset at 1843 LST.

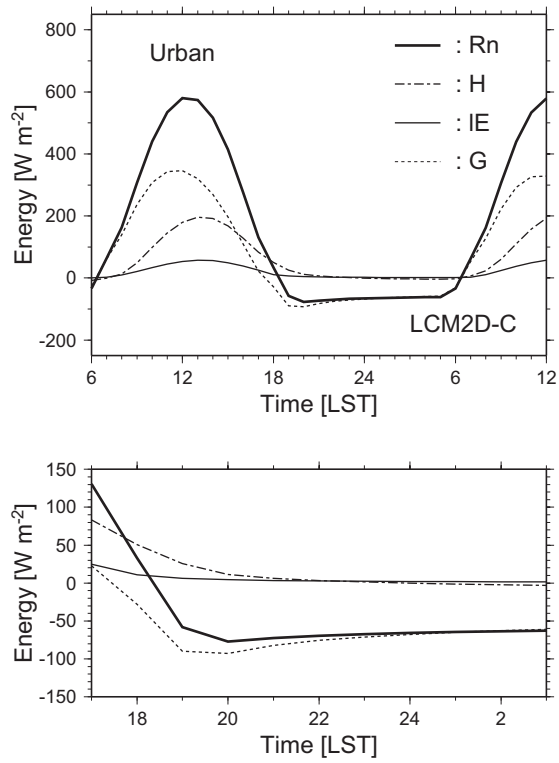

Fig. 8. Surface energy balance at the urban site from LCM2D-C. The thick solid line is net radiation, the dashed-and-dotted line is the sensible heat flux, the thin solid line is the latent heat flux, and the dashed line is the heat flux into the ground. Net radiation is positive when directed downwards to the surface. Sensible heat and latent heat fluxes are positive when directed upward, while the heat flux into the ground is positive when directed downward. Sunrise is at 0517 LST and Sunset at 1843 LST.

ban and rural sites. One of the major differences is that the latent heat flux is much smaller during the daytime at the urban site, indicating that the urban surface has less moisture than the rural surface due to smaller grass land. Persistence of the daytime heating by the warmer urban surface associated with small latent, and large sensible heat fluxes, helps produce and maintain the heat island and the circulation shown in Fig. 5. Another difference is that the heat flux into the ground is much larger during the daytime at the urban site, and thus the sensible heat flux remains positive until midnight at the warmer urban surface. This maintains the mixed layer near the surface, and produces the nocturnal heat island shown in Fig. 6. Duration of the heating depends on the canyon geometry, scale, location, weather conditions, season, and human activity (e.g., Oke 1981, 1987; Yoshikado 1994; Yoshino and Yamashita 1998; Ichinose et al. 1999; Sugawara 2001). However, observations show that the heating during the several hours after sunset is important, and essential feature of the urban heat island (e.g., Cleugh and Oke 1986; Grimmond and Oke 1995), which is not reproduced by LCM2D (Fig. 10). This indicates that the canopy processes in the LCM2D-C play a significant role for the mesoscale nocturnal heat island formation, through the modification of the surface heat budget in the urban areas.

4. Remarks

In this study, only LCM2D-C simulated the features of the urban heat budget that produces the nocturnal heat island phenomena where the urban surface is warmer than the rural surface at night. This implies that the urban canopy processes incorporated in this model are important for the nocturnal heat island.

We reconsider the different concepts between the slab urban model, and the single-layer ur-

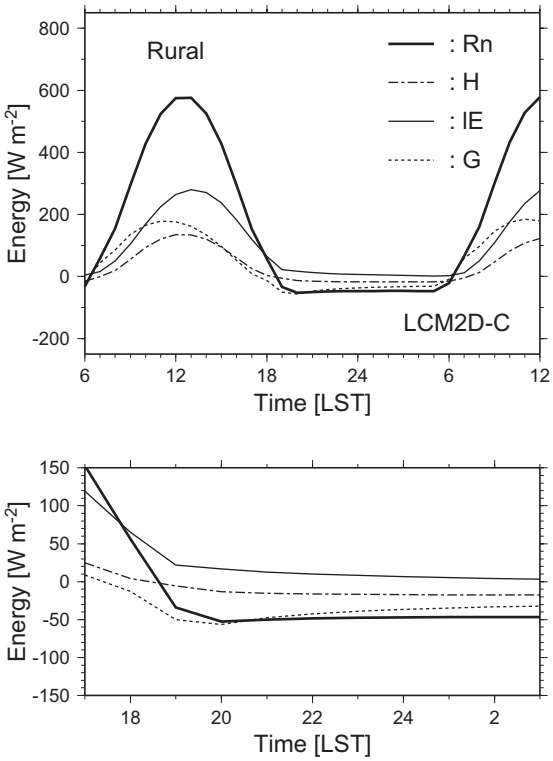

Fig. 9. Same as Fig. 8, but for the rural site.

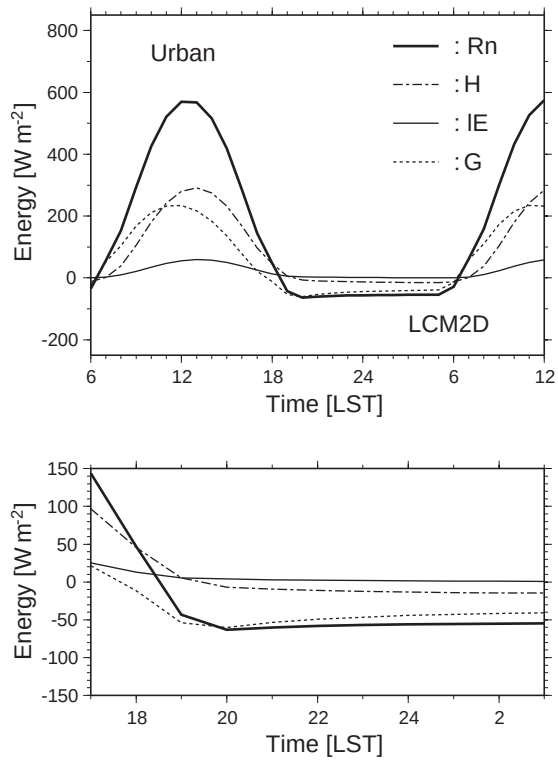

Fig. 10. Same as Fig. 8, but for LCM2D.

ban canopy model. One difference is that the single-layer urban canopy model has a larger volumetric heat capacity and a smaller sky view factor due to the existence of a vertical urban surface (Table 2). These factors are important for the phase, and diurnal range of the surface air temperature. Another difference between the two models must be the ratio of the effective aerodynamic resistances to the transfer of heat.

Oke (1981) pointed out that city with small sky viewer factor produces stronger nocturnal heat island intensity from the observations and the experiments using his scale model. Oke et al. (1991) and Kobayashi and Takamura (1994) theoretically calculated the upward long wave radiation flux from urban canyons, and confirmed that smaller sky view factor produced smaller upward long wave radiation flux. This implies canyon structure with small sky view factor keeps higher surface temperature during the night. Sugawara et al. (2001) observed radiometric surface temperature and estimated the thermal inertia, $\rho c \lambda$ from the cooling rate of the temperature after sunset. Their results show that the effective thermal inertia of the town scale is two to four times larger than that of the urban surface materials such as concrete

Table 2. Concept of the single-layer urban canopy model and slab urban model.

	Single-Layer Urban Canopy Model	Slab Urban Model
Heat Capacity	Construction materials Increased surface area	Construction materials
Shortwave Radiation	Reflection in the canopy	Effective surface albedo
Longwave Radiation	Reflection in the canopy	
Flux temperature	Canopy air temperature	Radiative temperature
Wind Speed	Weak canopy flow	

and asphalt. They point out that the difference in the thermal inertia between their estimation and the materials, is caused by the canopy structure with buildings. Kondo et al. (1999) shows that taller buildings causes smaller diurnal range of the canopy-layer air temperature using their multi-layer urban canopy model. Their results indicate the canopy structure makes the decrease of the daytime temperature and increase of the nocturnal temperature. The results in this study strongly support the importance of the canopy structure for the heat island formation suggested by the previous studies.

In the present study, 2 days simulations were conducted to investigate the effects of the single-layer urban canopy model on a heat island simulation. Some may suspect that the heat storage of buildings and roads accumulates, and as a consequence daytime temperature increases after running the model for several days. In nature, large-scale winds periodically advect the heat, and consequently produce the typical atmospheric condition like an initial condition assumed in the present study. Thus, the heat island circulation could be stronger after running the model for several days because such an effect could not be included in the model. However, the conclusions from the longer simulation should not basically differ from the current ones. This is because the daily mean of the heat storage is much smaller than that of the daytime heat release. In addition, the basic feature of the heat budget from the present 2 days simulation is similar to that from 5 days off-line simulation by Kusaka et al. (2001). The effects of the proposed urban canopy model on a longer simulation like a climate will be investigated in the future studies.

Tuning parameters of the slab urban model could decrease the discrepancy, but any such tuning should have a physical basis for estimating the individual factors. The tuning heat capacity and Stanton number (e.g., Sugawara et al. 2001) will be one of the subjects in the future studies.

5. Conclusions

The urban canopy-layer model was incorporated into the two-dimensional atmospheric model to determine its impact on the local circulation and heat island.

We found that the heat island circulation developed less strongly than when using the atmospheric model with the standard slab urban model.

The incorporation of the single-layer urban canopy model tends to reduce the diurnal variation of the surface air temperature and to delay the phase. It causes a 1°C lower daytime temperature, and a 4°C higher nocturnal temperature when the building height is 6 m and coverage ratio is 30%. The coupled model produces a linear drop in the temperature with time, and maintains a nocturnal heat island which results from the difference of the atmospheric stability between city and its surroundings.

We focused on the idealized summer case using the simple two-dimensional atmospheric model. The coupled technique used in this study was shown to be a very valuable one to study mesoscale heat island. The present results will be useful when doing simulations using complex three-dimensional mesoscale models with urban models. The procedure will be repeated for the various, more realistic land-cover and atmospheric conditions, and the results will be presented in a future study.

Acknowledgments

We thank Prof. Tetsuzo Yasunari of Nagoya University, Prof. Hiroshi L. Tanaka of University of Tsukuba and Adjunct Prof. Akio Kitoh of Meteorological Research Institute for their comments. We thank Dr. Hiromaru Hirakuchi, Dr. Nobukazu Tanaka, and Dr. Yoshikatsu Yoshida of the Central Research Institute of Electric Power Industry for their support. Special thanks go to Dr. Fei Chen, Ms. Kyoko Ikeda and Ms. Abena Poku-Awuah of the National Center for Atmospheric Research for their reviews and comments of an earlier version of this paper. Free software GMT (Generic Mapping Tools) was used in drawing the figures.

Appendix A

List of symbols for LCM

f	Coriolis parameter,
g	acceleration of gravity,
k	Von Karman constant,
K_H	horizontal exchange coefficient,

K_m vertical exchange coefficient of momentum,
K_h vertical exchange coefficient of heat,
q_v specific humidity,
Q_{RCOOL} radiative cooling rate,
t time,
T temperature,
T_R radiative temperature,
u east-west component of wind velocity,
u_G east-west component of geostrophic wind velocity,
v north-south component of wind velocity,
v_G north-south component of geostrophic wind velocity,
w vertical component of wind velocity,
θ potential temperature,
θ' $= \theta - \Theta$,
Θ mean potential temperature,
π Exner's function,
π' $= \pi - \Pi$,
Π mean Exner's function,
ρ_0 mean fluid density,

Apendix B

Single-layer urban canopy model

B.1 Short wave radiation flux

The effects of the shadows on the Lambertian surface are included in the model. The normalized shadow l_{shadow} on the road is defined as

$$l_{shadow} = \begin{cases} h_c \tan\theta_z \sin\theta_n & (l_{shadow} < l_{road}) \\ l_{road} & (l_{shadow} > l_{road}) \end{cases}. \tag{B.1}$$

Here, θ_z is the solar zenith angle. θ_n is the angle that forms when directions of sun and canyon axis are drawn from the same end points, and its magnitude is equal to the difference between the solar azimuth angle and canyon orientation. The net amount that is absorbed by the roof, wall, and road are calculated from (refer to Fig. 2).

$$S_R = S_D(1-\alpha_R) + S_Q(1-\alpha_R), \tag{B.2}$$

$$S_{W,1} = S_D \frac{l_{shadow}}{2h_c}(1-\alpha_W) + S_Q F_{W\to S}(1-\alpha_W), \tag{B.3}$$

$$\begin{aligned} S_{W,2} = {} & S_D \frac{l_{road} - l_{shadow}}{l_{road}} \alpha_G F_{W\to G}(1-\alpha_W) \\ & + S_Q F_{G\to S} \alpha_G F_{W\to G}(1-\alpha_W) \\ & + S_D \frac{l_{shadow}}{2h_c} \alpha_W F_{W\to W}(1-\alpha_W) \\ & + S_Q F_{W\to S} \alpha_W F_{W\to W}(1-\alpha_W), \end{aligned} \tag{B.4}$$

$$\begin{aligned} S_{G,1} = {} & S_D \frac{l_{road} - l_{shadow}}{l_{road}}(1-\alpha_G) \\ & + S_Q F_{G\to S}(1-\alpha_G), \end{aligned} \tag{B.5}$$

and

$$\begin{aligned} S_{G,2} = {} & S_D \frac{l_{shadow}}{2h_c} \alpha_W F_{G\to W}(1-\alpha_G) \\ & + S_Q F_{W\to S} \alpha_W F_{G\to W}(1-\alpha_G) \end{aligned} \tag{B.6}$$

The solar radiation is positive when directed towards the surface. S_D and S_Q are the direct solar radiation and the diffuse solar radiation received by a horizontal surface, respectively; the subscripts 1 and 2 refer to the absorption of the direct and reflected radiation, respectively; the subscripts W, G, and S denote wall, ground (road), and sky, respectively. The view factors F are also computed in the same way as Kusaka et al. (2001). The total direct solar radiation to a roof, wall, and road in a grid element is evaluated by the weighted average according to the relative area of different canyons. In other ward, net solar radiations for roof, wall, and road surfaces are average of the net radiations for each canyons that the user defined. Diffuse solar and downward long wave radiation are assumed to be emitted from the entire sky; i.e., it is assumed isotropic.

B.2 Long wave radiation flux

The net longwave fluxes absorbed by the roof, wall, and road surfaces are calculated from

$$L_R = \varepsilon_R(L^{\downarrow} - \sigma T_R^4), \tag{B.7}$$

$$\begin{aligned} L_{W,1} = {} & \varepsilon_W(L^{\downarrow} F_{W\to S} + \varepsilon_G \sigma T_G^4 F_{W\to G} \\ & + \varepsilon_W \sigma T_W^4 F_{W\to W} - \sigma T_W^4), \end{aligned} \tag{B.8}$$

$$\begin{aligned} L_{W,2} = {} & \varepsilon_W[(1-\varepsilon_G) L^{\downarrow} F_{G\to S} F_{W\to G} \\ & + (1-\varepsilon_G)\varepsilon_W \sigma T_W^4 F_{G\to W} F_{W\to G} \\ & + (1-\varepsilon_W) L^{\downarrow} F_{W\to S} F_{W\to W} \\ & + (1-\varepsilon_W)\varepsilon_G \sigma T_G^4 F_{W\to G} F_{W\to W} \\ & + \varepsilon_W(1-\varepsilon_W)\sigma T_W^4 F_{W\to W} F_{W\to W}], \end{aligned} \tag{B.9}$$

$$L_{G,1} = \varepsilon_G[L^{\downarrow} F_{G\to S} + \varepsilon_W \sigma T_W^4 F_{G\to W} - \sigma T_G^4], \tag{B.10}$$

and

$$L_{G,2} = \varepsilon_G[(1-\varepsilon_W)L^{\downarrow}F_{W\to S}F_{G\to W} + (1-\varepsilon_W)\varepsilon_G\sigma T_G^4 F_{W\to G}F_{G\to W} + \varepsilon_W(1-\varepsilon_W)\sigma T_W^4 F_{W\to W}F_{G\to W}]. \quad (B.11)$$

Here $L^{\downarrow}$ is the downward atmospheric long wave radiation; T_R, T_W, and T_G, are surface temperatures of the roof, wall, and road, respectively, and subscripts 1 and 2 refer to the absorption of the direct and reflected radiation, respectively.

B.3 Heat and momentumfluxes

Sensible heat flux from the building roof, building wall, and road is estimated at each surface individually. The sensible heat fluxes from the wall and road are calculated using the Jurges formula:

$$H_W = C_W(T_W - T_S), \quad (B.12)$$

$$H_G = C_G(T_G - T_S), \quad (B.13)$$

and

$$C_W = C_G = \begin{cases} 7.51U_S^{0.78} & (U_S \geq 5\ \mathrm{ms}^{-1}) \\ 6.15 + 4.18U_S & (U_S < 5\ \mathrm{ms}^{-1}) \end{cases}. \quad (B.14)$$

Note that Monin-Obukhov similarity theory is used under stable atmospheric condition for avoiding the problem about the Jurges formula.

The momentum, sensible heat, and latent heat exchanges between the canyon space and the overlaying atmosphere are the flux through the canyon top, using Monin-Obukhov similarity theory. In summary,

$$\tau = -\rho\frac{k^2}{\Psi_m(\zeta)^2}, \quad (B.15)$$

$$H = -\rho_0 c_p(\theta - \theta_S)\frac{ku_*}{\Psi_h(\zeta)}, \quad (B.16)$$

and

$$lE = -\rho_0 l(q_v - q_{vs})\frac{ku_*}{\Psi_h(\zeta)}. \quad (B.17)$$

Here q_{vs} is the specific humidity at $z_T + d$. Ψ_m and Ψ_h are the integrated non-dimensional shear function.

$$\Psi_m = \int_{\zeta_0}^{\zeta}\frac{\phi_m}{\zeta'}d\zeta', \quad (B.18)$$

$$\Psi_h = \int_{\zeta_T}^{\zeta}\frac{\phi_h}{\zeta'}d\zeta'. \quad (B.19)$$

Here, $\zeta_0 = z_0/L$, $\zeta_T = z_T/L$, and $\zeta = (z_a - d)/L$, and L is the Monin-Obukhov stability length:

$$L = -\frac{\rho c_p u_*^3\Theta}{kgH_A}, \quad (B.20)$$

where Θ is the mean temperature, z_T is the roughness length for heat. Although L is from an implicit equation under unstable conditions, it can be computed by iterations using the Newton-Rapson method. H_A is sensible heat flux from artificial surface. The non-dimensional shear functions of Dyer and Hicks (1970) for unstable conditions and Kondo et al. (1978) for stable conditions. Note that the upper limit of integration for non-dimensional shear functions is $\zeta = (z_a - d)/L$, and surface temperature for this scheme is canyon air one defined at the height of $z_T + d$. This scheme is also applied for the fluxes from the roof.

The air within the urban canopy-layer has a negligible heat capacity and so sensible heat flux from the building wall H_W, and from the road H_G, must be balanced by the sensible heat flux to the atmosphere from the canyon space, i.e.,

$$l_{road}H_a = 2h_c H_W + l_{road}H_G. \quad (B.21)$$

The total heat flux to the atmosphere from the urban area is the area-weighted average from the roof and that through the canyon top. If the ground surface in a grid area is classified into artificial and vegetated surfaces with area ratios A_A and A_V, respectively, the total heat fluxes at the grid points are the averaged heat fluxes on the artificial and vegetated surfaces weighted by their area (Kimura 1989). The modified equation is

$$H = A_A H_A + A_V H_V = A_A[l_{roof}H_R + l_{road}H_a] + A_V H_V, \quad (B.22)$$

where, heat flux from the vegetation surface H_V can be estimated from a vegetation model (The standard slab grassland model is used in the present study).

B.4 Wind speed within canopy

The mean wind speed in the canopy layer is used as a reference to calculate H_G and H_W. Within canopy layer, buildings are usually dif-

fusely distributed and act as a continuum-like sink for momentum. Under such conditions the mean wind speed and shearing stress should decay with depth below the canopy top. In the present model, the stress divergence in the air is assumed to balance the drag per unit volume of air,

$$-\frac{\partial}{\partial z}\left(\gamma_V K_m \frac{\partial U}{\partial z}\right) - \gamma_V c_d a_z U = 0, \qquad \text{(B.23)}$$

where eddy viscosity model is used. The a_z is the function of height and equal to the surface area of buildings per unit volume of air, and c_d is a drag coefficient. The γ_V is the effective fluid volume (Kondo et al. 1999). The present study uses the assumptions on the constant mixing length l, and drag coefficient in the canopy layer by Inoue (1963). The result is an exponential wind profile given by

$$U = U_a \frac{\log[(z_a - d)/z_0]}{\log[(z_r - d)/z_0]} \exp[-n(1 - z/z_r)]. \qquad \text{(B.24)}$$

Here, $n = (c_d a_z/2l^2)^{1/3}$. In fact, wind profiles within an urban canopy from filed observations and numerical simulations are exponential (e.g., Nicholson 1975; Depaul and Sheiht 1986; Maruyama 1999).

References

Avissar, R., 1996: Potential effects of vegetation on the urban thermal environment. *Atmos. Environ.*, **30**, 437–448.

——— and R.A. Pielke, 1989: A parameterization of heterogeneous land-surface for atmospheric numerical models and its impact on regional meteorology. *Mon. Wea. Rev.*, **117**, 2113–2136.

Ca, V.T., Y. Ashie, and T. Asaeda, 2002: A k-ε turbulence closure model for the atmospheric boundary layer including urban canopy. *Bound.-Layer Meteor.*, **102**, 459–490.

Cleugh, H.A. and T.R. Oke, 1986: Suburban-rural energy balance comparisons in summer for Vancouver, B.C.. *Bound.-Layer Meteor.*, **36**, 351–369.

Depaul, F.T. and C.M. Sheih, 1986: Measurements of wind velocities in a street canyon. *Atmos. Environ.*, **20**, 455–459.

Dyer, A.J. and B.B. Hicks, 1970: Flux gradient relationship in the constant flux layer. *Quart. J. Roy. Meteor. Soc.*, **96**, 715–721.

Grimmond, C.S.B. and T.R. Oke, 1995: Comparison of heat fluxes from summertime observations in the suburbs of four North American cities. *J. Appl. Meteor.*, **34**, 873–889.

Inoue, E., 1963: On the turbulent structure of airflow within crop canopies. *J. Meteor. Soc. Japan*, **41**, 317–326.

Ichinose, T., K. Shimodozono, and K. Hanaki, 1999: Impact of anthropogenic heat on urban climate in Tokyo. *Atmos. Environ.*, **33**, 3897–3909.

Kanda, M., Y. Inoue, and I. Uno, 2001: Numerical study on cloud lines over an urban street in Tokyo. *Bound.-Layer Meteor.*, **98**, 251–273.

Kimura, F., 1989: Heat flux on mixture of different land-use surface: Test of a new parameterization scheme. *J. Meteor. Soc. Japan*, **67**, 401–409.

——— and P. Manins, 1988: Blocking in periodic valleys. *Bound.-Layer Meteor.*, **44**, 137–169.

——— and S. Takahashi, 1991: The effects of land-use and anthropogenic heating on the surface temperature in the Tokyo metropolitan area: A Numerical experiment. *Atmos. Environ.*, **25B**, 155–164.

——— and T. Kuwagata, 1993: Thermally induced wind passing from plain to basin over a mountain range. *J. Appl. Meteor.*, **32**, 1538–1547.

——— and T. Kuwagata, 1995: Horizontal heat fluxes over complex terrain computed using a simple mixed layer model and a numerical model. *J. Appl. Meteor.*, **34**, 549–558.

Kobayashi, T. and T. Takamura, 1994: Upward longwave radiation from a non-black urban canopy. *Bound.-Layer Meteor.*, **69**, 201–213.

Kondo, H., Y. Kikegawa, Y. Genchi, and S. Yamamoto, 1999: Heating in the Urban Canopy by Anthropogenic Energy Use. *Proceedings of 15th International Congress of Biometeorology and International Conference on Urban Climatology (ICB-ICUC '99)*, Sydney, Australia, November 8–12, 1999, ICB-ICUC, in CD-ROM.

Kondo, J., O. Kanechika, and N. Yasuda, 1978: Heat and momentum transfers under strong stability in the atmospheric surface layer. *J. Atmos. Sci.*, **35**, 1012–1021.

Kusaka, H., F. Kimura, H. Hirakuchi, and M. Mizutori, 2000: The effects of land-use alteration on the sea breeze and daytime heat island in the Tokyo metropolitan area. *J. Meteor. Soc. Japan*, **78**, 405–420.

———, H. Kondo, Y. Kikegawa, and F. Kimura, 2001: A simple single-layer urban canopy model for atmospheric models: Comparison with multi-layer and slab models. *Bound.-Layer Meteor.*, **101**, 329–358.

Lee, S.H. and F. Kimura, 2001: Comparative studies in the local circulation induced by land-use and by topography. *Bound.-Layer Meteor.*, **101**, 157–182.

Maruyama, T., 1999: Surface and inlet boundary conditions for the simulation of turbulent boundary layer over complex rough surfaces. *J. Wind Eng. Ind. Aerodyn.*, **81**, 311–322.

Masson, V., 2000: A physically-based scheme for the urban energy budget in atmospheric models. *Bound.-Layer Meteor.*, **94**, 357–397.

Martilli, A., A. Clappier, and M.W. Rotach, 2002: An urban surface exchange parameterization for mesoscale models. *Bound.-Layer Meteor.*, **104**, 261–304.

Mellor, G.L. and T. Yamada, 1974: A hierarchy of turbulence closure models of planetary boundary layers. *J. Atmos. Sci.*, **31**, 1791–1806.

Mills, G.M., 1997: An urban canopy-layer climate model. *Theor. Appl. Climatol.*, **57**, 229–244.

Nicholson, S.E., 1975: A pollution model for street-level air. *Atmos. Environ.*, **9**, 19–31.

Ohashi, Y. and H. Kida, 2002a: Effects of mountain and urban areas on daytime local-circulations in the Osaka and Kyoto regions. *J. Meteor. Soc. Japan*, **41**, 30–45.

——— and H. Kida, 2002b: Numerical experiments on the weak-wind region formed ahead of the sea-breeze front. *J. Meteor. Soc. Japan*, **80**, 519–527.

Oke, T.R., 1981: Canyon geometry and nocturnal urban heat island: Comparison of scale model and field observations. *J. Climatol.*, **1**, 237–254.

———, 1987: *Boundary Layer Climates 2nd edn.* Methuen Co., London/New York, 435pp.

———, G.T. Jhonson, D.G. Steyn, and I.D. Watson, 1991: Simulation of surface urban heat islands under 'ideal' conditions at night.—Part 2: Diagnosis of causation. *Bound.-Layer Meteor.*, **56**, 339–358.

Sugawara, H., 2001: Heat exchange between urban structures and the atmospheric boundary layer. PhD thesis, Tohoku university.

———, K. Narita, and T. Mikami, 2001: Estimation of effective thermal property parameter on a heterogeneous urban surface. *J. Meteor. Soc. Japan*, **79**, 1169–1181.

Tanaka, S., H. Takeda, T. Adachi, and T. Tsuchiya, 1993: *Architectural Environmental Engineering*, Inoue Co., LTD., 301pp. (in Japanese).

Uno, I., H. Ueda, and S. Wakamatsu, 1989: Numerical modeling of the nocturnal urban boundary layer. *Bound.-Layer Meteor.*, **49**, 77–98.

———, X-M. Cai, D.G. Steyn, and S. Emori, 1995: A simple extension of the Louis method for rough surface layer modeling. *Bound.-Layer Meteor.*, **76**, 395–409.

Wessel, P. and W.H.F. Smith, 1995: New version of the Generic Mapping Tools released. *EOS Trans. Amer. Geophys. U.*, **76**, 329pp.

Yamamoto, G., A. Shimanuki, M. Aida, and N. Yasuda, 1973: Diurnal variation of wind and temperature fields in the Ekman layer. *J. Meteor. Soc. Japan*, **51**, 377–387.

Yoshikado, H., 1992: Numerical study of the daytime urban effect and its interaction with the sea breeze. *J. Appl. Meteor.*, **31**, 1146–1164.

———, 1994: Interaction of the sea breeze with urban heat islands of different size and locations. *J. Meteor. Soc. Japan*, **72**, 139–143.

Yoshino, M. and S. Yamashita, 1998: *Urban Environmental Encyclopedia.* Asakura press, Tokyo, (in Japanese).